Hindawi
Shock and Vibration
Volume 2021, Article ID 4497086, 10 pages
https://doi.org/10.1155/2021/4497086

Research Article

Hydrodynamic Performance of A-Jacks Concrete Armor Units in Riverbeds around Downstream in Flip Buckets

Kamran Khalifehei,[1] **Gholamreza Azizyan**,[1] **and Mahmood Shafai-Bajestan**[2]

[1]*Department of Civil Engineering, University of Sistan and Baluchestan, Zahedan 987-98155, Iran*
[2]*Department of Hydraulic Structures, Faculty of Water Science Engineering, Shahid Chamran University of Ahvaz, Ahwaz, Iran*

Correspondence should be addressed to Kamran Khalifehei; kamran.khalifehei@pgs.usb.ac.ir

Received 3 July 2021; Revised 28 July 2021; Accepted 5 August 2021; Published 12 August 2021

Academic Editor: S. Mahdi S. Kolbadi

The jet flipped from flip buckets hits the dam's downstream side as a free jet with an immense amount of energy, leading to bed erosion. Erosion of river bed materials downstream of dams could affect the performance of dams or power plants by altering the tailwater depth, rendering proper designs of controlling structures or erosion reduction methods highly indispensable in this regard. Hence, the hydrodynamic performance of A-Jacks concrete armor units in controlling scour was examined in this study. A-Jacks armors are applicable as a flexible protection without environmental risks often for bed erosion control. The desirable functionality of A-Jacks armors depends on the flow hydrodynamic parameters such as velocity profile variations (U/U_B), the Reynolds stresses ($\tau_{u'w'}$ and $\tau_{v_t w_t}$), and the skin friction coefficient (C_f) created as a consequence of using A-Jacks armors on beds. The size of A-Jacks elements can have a role in increasing the flow turbulence to a certain depth so that after the impact of the flow with A-Jacks armor, the vortices' intensity as well as the shear stress affecting the bed gradually decreases. The results of the numerical model suggest that the surge in the flow turbulence energy dissipation downstream of flip buckets significantly mitigates the underlying conditions of scouring phenomena, which is evidence of A-Jacks armors' acceptable performance in scaling down scour depths.

1. Introduction

Use of A-Jacks concrete armor units represents one of the simplest and most practical systems protecting erodible beds. These six-legged elements are designed to create a solid material when the legs are interlocked. Hence, lighter elements than riprap are required. On the other hand, the ridges in piers and roughness formation cause the inlet jet flow to break down into smaller jets, and more importantly, the roughness leads to an increase in the shear force and energy dissipation. Furthermore, a part of the original jet infiltrates the elements and the bed, and it is likely to develop bed sour. Therefore, the number of layers placed on top of each other has an effect on scour depth as well [1]. A blend of A-Jacks armors and riprap could help reduce the scour dimensions. In such an occasion, the armors and the riprap will be smaller in size and also more convenient and economic to implement. Figure 1 illustrates the design of A-Jacks armors and their use in river engineering and hydraulic engineering.

A-Jacks armors have been incorporated in marine structures such as breakwaters and coast protections. In addition to the extensive applications of these elements in marine structures, their use in controlling river bank erosions has also attracted much attention recently [2]. A review of the available resources indicates that only a highly limited number of studies have addressed A-Jacks armors from structural and hydraulic points of view in general. The hydraulic studies available on A-Jacks elements are very limited and related to protecting sea coasts, piers, and bridge abutments. One of the most important studies investigating, from the structural viewpoint, the elements' buckling under vertical static loads was carried out by Mickel [3].

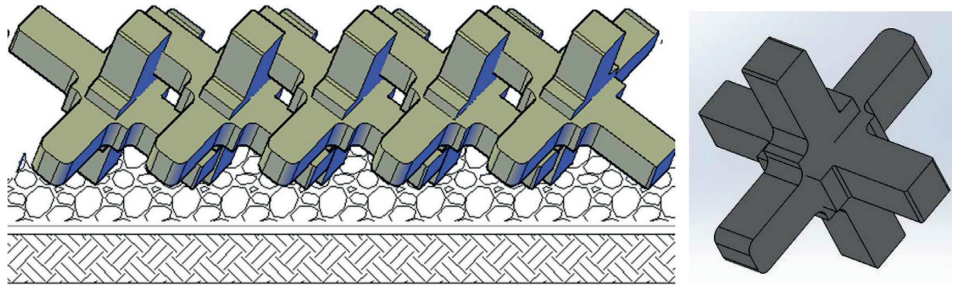

Figure 1: .Geometric shape of six-legged elements and an instance of A-Jacks armors' interlock.

Latta [4] also conducted other studies on six-legged concrete elements in hydraulic structures, and these studies include physical and numerical simulations of the elements, and analysis of the applied forces as well as the elements' stability.

As for the other hydrodynamic studies on A-Jacks armors, the two-step report put forth by the Soil and Water Conservation Bureau of the United States at Manly Hydraulics Laboratory could be stated as a study carried out with the purpose of comparing and assessing six-legged components against different breakwater components experimentally and modifying those designs [1]. In the experiments conducted by Thornton et al. on bridge pier scour hole control on a sand bed using A-Jacks armors, the decrease in the scour depth values after using these elements has been reported to be 70 to 95%, and for gaining more efficiency from these elements, use of geotextile filters with them has been recommended [2]. Zolghadr et al. demonstrated that installation of A-Jacks armors could control scouring at the trapezoidal crest up to 100%. Extensive research has been undertaken in Shahid Chamran University in order to examine application of six-legged elements for protecting the stilling basins' bed, indicating that a proper arrangement of these elements could reduce the stilling basin at length and the conjugate depth as well as scour depth downstream of the basins [5, 6]. Hosein Reza et al. applied the combined method of utilizing both ripraps and six-legged elements as direct methods of controlling scour at a rectangular abutment. As reported in the results of their tests, the combined implementation of riprap and six-legged elements had a significant effect [7]. Khalifehei et al. investigated A-Jack armors' stability on the erodible bed downstream of flip buckets and proposed a design for these armors [8, 9].

In their studies, Nou et al. examined the efficiency of six-legged concrete elements in controlling scour downstream of flip bucket spillways by conducting experimental studies. Their work addresses sediment scour hole volume reduction with simultaneous presence of six-legged concrete elements, under the brand of A-Jack, and riprap downstream of a flip bucket spillway under different hydraulic conditions of the flow. The results suggest that an increase in the tailwater depth significantly mitigated scouring, and the simultaneous presence of the concrete element and riprap could cause up to 100% drop in the maximum scour volume among various hydraulic conditions in comparison with that in the control test [10, 11].

A-Jacks advantages, such as their interlocking capability, their applicability in regions lacking appropriate rocks, and the possibility of vegetation's growing between the units, can help the armor's stability under certain conditions. On the other hand, the present study is deemed necessary as there have been no works available investigating the flow hydrodynamic parameters on these armors using numerical methods so far. Accordingly, this study embarks on simulation of A-Jacks armors implemented downstream of flip bucket spillways as a method of scouring control as a new and widely applicable topic in hydraulic engineering.

2. Theoretical Approach

The Flow3D model is applicable for analyzing unsteady 3D flows with a free surface and a complex geometry. The finite volume method is used in this numerical model in an orderly rectangular cell grid. Two methods have been used in this numerical model for geometric simulation. The first method is Volume of Fluid (VOF), which is incorporated to demonstrate the fluid behavior at the free surface. The second method is called Fractional Area/Volume Obstacle Representation (FAVOR), which is applied for simulation of surfaces and rigid volumes such as geometric boundaries [12–14].

The equations governing the fluid flow are extracted from the principles of mass conservation and momentum conservation and are represented as partial differential equations. The main equations for simulating the three-dimensional flow are three differential equations including the continuity and momentum equations in x, y, and z directions. The flow continuity equation is extracted from the principle of mass conservation and by writing the balance relation for a fluid element. The general continuity equation is presented as follows:

$$V_f \frac{\partial \rho}{\partial t} + \frac{\partial}{\partial x}\left(\rho u A_x\right) + \frac{\partial}{\partial y}\left(\rho v A_y\right) + \frac{\partial}{\partial z}\left(\rho w A_z\right) = 0, \quad (1)$$

where v_f is the fraction of volume to flow and ρ is the fluid density. Velocity components (u, v, w) are in x, y, and z directions. A_x is the fraction of free surface in x direction, and A_y and A_z are similarly fractions of surface in y and z directions.

The fluid's motion equations with velocity components (u, v, w) in three directions in coordinates, i.e., the Navier–Stokes equations, are presented as follows:

$$\frac{\partial u}{\partial t} + \frac{1}{V_F}\left(uA_x\frac{\partial u}{\partial x} + vA_y\frac{\partial u}{\partial y} + wA_z\frac{\partial u}{\partial z}\right) = -\frac{1}{\rho}\frac{\partial p}{\partial x},$$
$$\frac{\partial v}{\partial t} + \frac{1}{V_F}\left(uA_x\frac{\partial v}{\partial x} + vA_y\frac{\partial v}{\partial y} + wA_z\frac{\partial v}{\partial z}\right) = -\frac{1}{\rho}\frac{\partial p}{\partial y}, \quad (2)$$
$$\frac{\partial w}{\partial t} + \frac{1}{V_F}\left(uA_x\frac{\partial w}{\partial x} + vA_y\frac{\partial w}{\partial y} + wA_z\frac{\partial w}{\partial z}\right) = -\frac{1}{\rho}\frac{\partial p}{\partial z},$$

where G_x, G_y, and G_z denote mass accelerations and f_x, f_y, and f_z are viscosity accelerations.

The Flow3D numerical model is used for simulating transport, erosion, deposition, and static position of the nonadhesive sediments under the influence of the fluid flow. The sediment model of this numerical model uses two concentration fields: (1) floating nonadhesive sediments and (2) bed nonadhesive sediments.

Displacement and lifting of floating sediments with the fluid occur due to variations in the local pressure gradient. These floating nonadhesive sediments could be a result of the inlet flow containing floating particles or stem from bed erosion. Since bed sediments are restricted by the adjacent particles and cannot move easily, they can get in motion if they are converted into floating load as eroded particles at the interface between the bed and the fluid, and the floating load can convert into bed load in case the deposition velocity is higher than the bed erosion velocity [15, 16]. A part of the control volume, occupied by solid sediment particles, is denoted by f_S, and the rest made of accumulated fluid is defined by f_L; therefore,

$$f_S + f_L = 1. \quad (3)$$

The floating load increases the real fluid viscosity. Such an increase lasts until the volume fraction of the solid particles reaches the limit of the volume fraction of viscosity. After that the increase in the floating load does not cause a higher viscosity but results in the particle's growing active in a solid manner. In this case, the average fluid viscosity is obtained as follows:

$$\mu^* = \mu_f\left(1 - \frac{\mathrm{Min}\left(f_S, f_{sco}\right)}{f_{sCR}}\right), \quad (4)$$

where μ_f represents the fluid viscosity and μ^* is the average viscosity of the critical fraction of nonadhesive sediments particles. The perceived density, $\overline{\rho}$, is assumed as a linear function of the sediments volume, where ρ_s and ρ_L are the apparent densities of the sediment and the fluid [17].

Drift is defined as sediment particles deposition under the influence of the drift forces affecting the sediment particle. In the sediment washing model in the Flow3D numerical model, the sediment particles are assumed spherical so that they are influenced by the fluid viscosity; hence, deposition is automatically calculated according to the following relation:

$$D_f = \frac{d_{50}^2 \times (\rho_s - \rho_L)}{18\mu}. \quad (5)$$

Therefore, the deposition velocity is obtained as follows:

$$u_{\mathrm{drift}} = D_f \times f_L\frac{\nabla P}{\overline{\rho}} = \frac{f_L \times d_{50}^2}{18\mu}\frac{\nabla P}{\overline{\rho}}(\rho_s - \rho_L), \quad (6)$$

where $\nabla P/\overline{\rho}$ is defined as the gradient of mechanical potential or acceleration and is limited to 10 times the particle's weight, leading to elimination of numerical fluctuations in the amount of pressure. Near the fluid free surface, the value of $\nabla P/\overline{\rho}$ is replaced by g. The f_L coefficient is included in equation (6) because sedimentation is possible only with the presence of solid particles (sediment) [18, 19]. Therefore, if the control volume is filled with sediment, then $f_L = 0$ and thus $u_{\mathrm{drift}} = 0$. The shear stress is active at the bed sediment level, which leads to erosion and displacement of nonadhesive sediments at bed surface. This erosion is a function of the fluid shear stress at surface, the critical shear stress, and the fluid and sediment densities. The critical Shields parameter represents the minimum shear stress required for lifting sediment particles from the interface between the fluid and the active bed.

$$\theta_{\mathrm{cirt}} = \frac{\tau_{\mathrm{crit}}}{g(\rho_L - \rho_s)d}, \quad (7)$$

where θ_{cirt} is the critical Shields parameter and τ_{crit} denotes the minimum shear stress required along the bed to lift sediment particles. Elaborating on and describing this model is aimed to estimate and predict the amount of sediment flow eroded over the shared bed. To this end, the shear velocity parameter is defined for measuring the flow power in bed erosion [20, 21]. Hence, the rate of sediment lift from the bed could be presented as follows:

$$U_{\mathrm{lift}} = \alpha n_s\sqrt{\frac{\tau - \tau_{\mathrm{crit}}}{\overline{\rho}}}, \quad (8)$$

where n_s is the bed surface normal vector and α represents the dimensionless parameter which shows the possibility of sediment particles' being lifted from the bed, which is usually less than or equal to unity. In a static fluid, the internal friction angle of sediment particles determines the minimum slope at which sediment walls can be stable. A high internal friction angle of sediments, as in clay, implies stability of the wall at sharp slopes, and a low internal friction angle, as in sand, demonstrates a high inclination for slump and forward motion. At the downstream side of the hole, where sediments are piled up and make a bulk of sediments, the state of sediment position creates a horizontal angle which represents the internal friction angle. In the model, ξ denotes this angle. The natural angle of repose for sediments under different spatial and temporal conditions is calculated as follows:

$$\phi = \frac{n_{\text{interface}} \cdot g}{|g|}, \tag{9}$$

where $n_{\text{interface}}$ is equal to the surface normal vector and g is the acceleration of gravity. The critical shear stress which occurs at the sloped surface is calculated according to the following equation for each surface after the occurrence of scour or floating sediment transport at that surface:

$$\tau_{\text{crit}} = \tau^{0}_{\text{crit}} \sqrt{1 - \frac{\sin^2 \varphi}{\sin^2 \xi}}. \tag{10}$$

Based on equation (10), when the natural slope of the sediment is equal to its internal friction angle ($\phi = \zeta$), the critical shear stress will be equal to zero, i.e., the bed surface undergoes erosion owing to any type of shear stress applied. In addition, when $\phi > \zeta$, then $\tau_{\text{crit}} < 0$, i.e., the sediments undergo erosion even when there is no shear stress. The above relation also indicates that as large as the sediment particles' internal friction angle becomes, the wall slope ($\tau_{\text{crit}} = 0$) must also grow large so that the scour or flushing hole wall undergoes erosion without the presence of shear stress (ϕ). Transport of the sediment floating in the system is stated by the convection-diffusion equation [22, 23].

$$U_j \frac{\partial c_s}{\partial x_j} - \omega_s \left(\frac{\partial c_s}{\partial z} \right) = \frac{\partial}{\partial x_j} \left(\Gamma \frac{\partial c_s}{\partial x_j} \right), \tag{11}$$

where c_s is the sediment concentration, Γ denotes the diffusion coefficient, and ω_s is the particles settling velocity as follows:

$$\omega_s = u_{\text{lift}} - u_{\text{drift}}. \tag{12}$$

As a result, equation (12) enters the solution according to the following:

$$\frac{\partial c_s}{\partial t} + u \cdot \nabla c_s = \Gamma \nabla^2 c_s - u_{\text{lift}} \cdot \nabla c_s - u_{\text{drift}} \cdot \nabla c_s. \tag{13}$$

The concentration of the floating sediment at the interface between nonadhesive sediments bed and water prior to the onset of flushing ($t = 0$) is obtained as follows:

$$C_{so} = f_s * \rho. \tag{14}$$

The above relations and computational algorithm are used in the Flow3D numerical model in order to drain bed sediments. In the following numerical model, the flow hydrodynamic parameters will be addressed using the proposed theoretical approach. For geometric simulation, two strategies were applied in this numerical model. Volume of Fluid (VOF) is the initial method, which is used to demonstrate fluid dynamics at the free surface. The second method, known as FAVOR (Fractional Area/Volume Obstacle Representation), is used to simulate surfaces and rigid volumes such as geometric bounds.

3. Research Method

In every simulation carried out in this study, the 3D flow field has been solved using the RNG turbulence model. The RNG model was developed using Renormalisation Group (RNG) methods by Yakhot et al. to renormalise the Navier–Stokes equations, to account for the effects of smaller scales of motion. In the standard k-epsilon model, the eddy viscosity is determined from a single turbulence length scale, so the calculated turbulent diffusion is that which occurs only at the specified scale, whereas in reality, all scales of motion will contribute to the turbulent diffusion. The RNG approach, which is a mathematical technique that can be used to derive a turbulence model similar to the k-epsilon, results in a modified form of the epsilon equation which attempts to account for the different scales of motion through changes to the production term [24, 25]. The reason for using this turbulence model can be attributed to its properties and advantages over models such as $k - \varepsilon$. This model has been improved due to having one ε extra term for analyzing quickly strained flows and the flows over surfaces with numerous geometric variations and is greatly capable in transient flow simulations [26]. In addition, relying on the comparison made between turbulence models over spillways using Flow3D conducted by Yamini (2018), the RNG turbulence model has had more accurate results than other turbulence models, and it has therefore been used in the present work [27, 28]. In this simulation, the flow over ogee spillways was modeled using real model data, and it was analytically solved. In addition, the fluid, nonviscous and incompressible, and the air inlet with a density of 1.24 kg/m^3 and a shear stress rate of 0.0731 were taken into consideration.

It is noteworthy that there are 898,287 computational cells considered for this simulation. Different boundary conditions have been assumed per the most appropriate channel length behind the spill way as 1 meter long water prior to the ogee spillway and inside the dam reservoir. As for the size, the elements utilized in the study are categorized into six classes named A-Jacks 1 to A-Jacks 6, and A-Jacks 1 size is provided in Figure 2. The other elements have also been designed and considered in order with 20% larger dimensions. Further, the boundary conditions of the flow simulation over ogee spillways are defined in Figure 2. Different conditions have been considered to apply boundary conditions to the mesh block (Figure 2). As for the inflow, the flow rate is applied along with the flow depth (Q). Outflow conditions (O) are considered in terms of output. The wall boundary condition (W) is applied to the lateral walls. The boundary condition of the wall (W) is applied on the bottom of the mesh block, and the boundary condition of symmetry (S) is considered on the roof of the mesh block. grid as wall and symmetry, the bed and top for computational cells as, respectively, wall and symmetry.

The first step in a numerical model is model calibration. This means minimizing the effect of external factors and maintaining model conditions more similarly to a real-world situation. The present numerical model has been done based on the experimental model; hence, its calibration and validation have been carried out accordingly. The calibration of the numerical model with respect to simulation and boundary conditions is discussed here. It is necessary to achieve stable conditions in order to extract accurate values

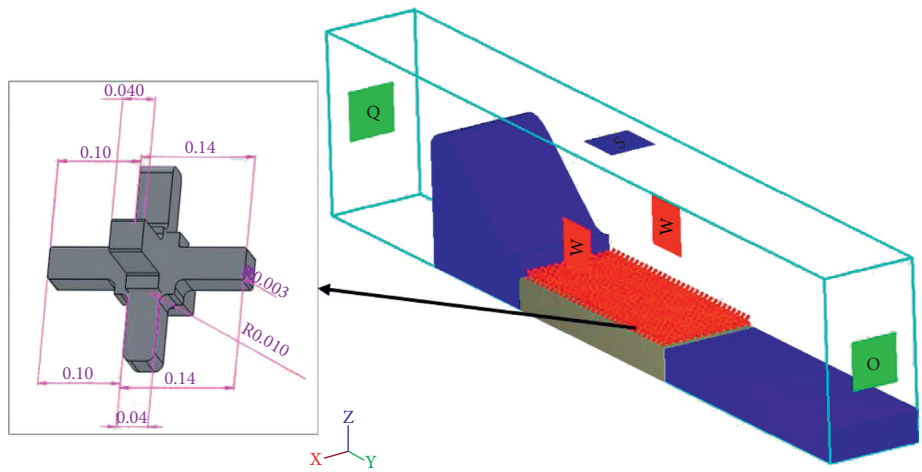

Figure 2: Boundary conditions applied to numerical modeling and geometric dimensions of A-Jacks 1 concrete block.

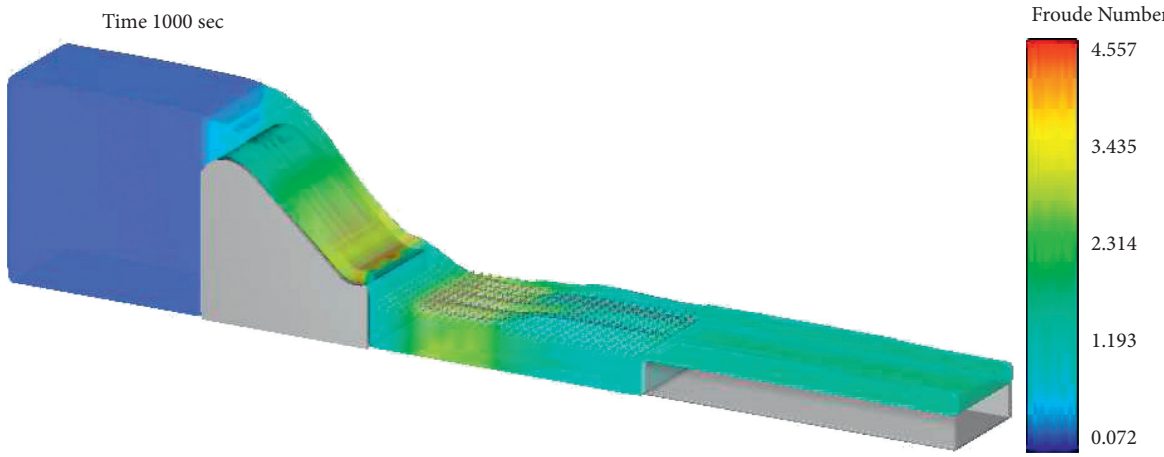

Figure 3: Flow development in the Flow3D numerical model.

from numerical or real-world model data. In the numerical model under investigation, the proper time for extracting the results from the model was considered 180 minutes after examining a number of models. Figure 3 illustrates how the flow passes over the spillway at different points in time. The flow becomes stable over the spillway and the downstream channel after 40 seconds.

At the onset of calculations for the numerical model ($T = 0.0$ sec), the fluid height was introduced in correspondence with the experimental data intended for the model. With the beginning of calculations by the software ($T = 1$ sec), the flow passes over a part of the ogee spillway. At $T = 5$ sec, the flow is led out from the ogee spillway. At $T = 10$ sec, the unsteadiness effect of the flow on the downstream channel is evident. Although the flow seems steady at $T = 15$–35 sec, more careful attention to the differences in the fluid fraction contours at the upcoming times reveals that the flow becomes steady from $T = 40$ sec. To ascertain the steadiness and equilibrium of the flow field over ogee spillways, the diagram on variations in the rate of flow passing inflow and outflow boundaries per time is presented, as in Figures 4 and 5, which indicate flow stability and steadiness after 40 seconds, which in turn confirms simulation stability. All analyzes of flow hydrodynamic parameters under stable flow conditions have been performed on a numerical model.

4. Results and Discussion

To study the effect of A-Jacks element sizes on the flow hydraulic parameters, 6 element sizes, whose geometric dimensions were increased by 20%, were placed on the erodible bed of the channel downstream of the ski-jump. Data collection stations are shown in Figure 6. The numerical model was run for each considering a constant flow rate, and the hydraulic parameters were analyzed. It should be noted that the hydraulic parameters for 9 downstream stations were evaluated as relative parameters (X/H).

Investigation of the flow velocity profile gains great significance in finding the pattern of the flow jet energy dissipation downstream of flip buckets. The profile variation trend from the onset of jet formation to the end of erodible locations indicates the manner of flow development and turbulence variations. In this section, after extraction of the numerical simulation results, a comparison of velocity

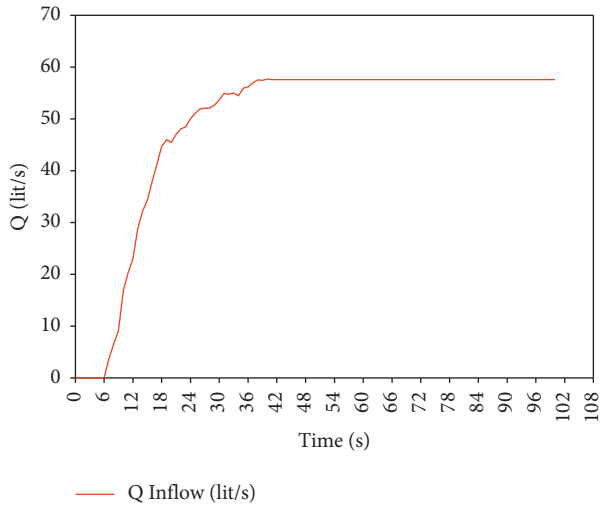

Figure 4: Flow rate variations at the inflow boundary in proportion to the time of running the numerical model.

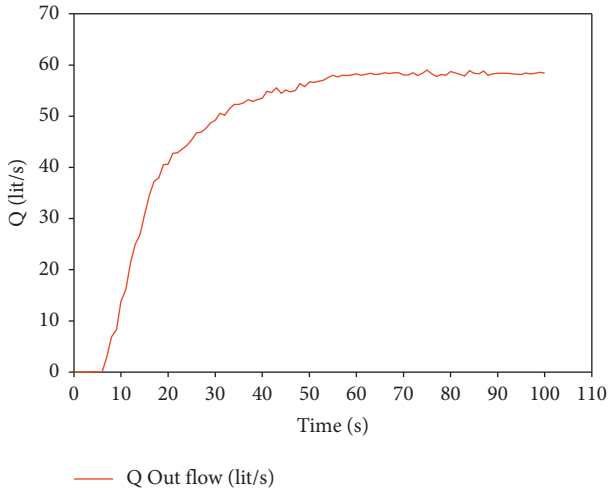

Figure 5: Flow rate variations at the outflow boundary in proportion to the time of running the numerical model.

profiles nondimensionalized in proportion to the flow velocity in the flip bucket (U/U_B) and for different stations with different sizes of A-Jacks element armors was provided.

As depicted in Figure 7, at station $X/L = 0$, which represents the flow jet point of inlet into the tailwater, variations in A-Jacks dimensions show little effect on velocity profiles. With the flow passing over the A-Jacks, the flow turbulence increases due to A-Jacks roughness. In other words, the roughness stemming from A-Jacks element's piers ($X/L = 0$) causes flow separation from bed and its return at station ($X/L = 1$). Presence of A-Jacks armors on bed generates a positive pressure gradient, leading to velocity reduction near the bed. Reduction in velocity gradients is highly evident for A-Jacks with larger dimensions, which indicates that the bed erodibility potential as a result of using larger armors could entail bed scour reduction. After the shear layer, velocity variations become almost constant towards the water surface, as seen in velocity profiles. This is because the flow structure at depths closer to the water surface is unaffected by the bed shape. Given that most flow scour holes occur in the region where the flow jet impacts the downstream side, using larger elements can strengthen velocity profiles towards increasing the flow turbulence and flow energy dissipation and make for more desirable conditions of the flow in this region. It is important to note that with the passage of flow into the downstream region, the elements' dimensions at regions farther away from the jet impact will have less effect owing to flow development and full formation of the boundary layer.

Since the Reynolds stress turbulence parameters have a number of transport terms and heterogeneous and non-isotropic diffusions in comparison with other turbulence parameters, they are more accurate and sensitive in energy transfer from the mean flow to fluctuating parameters. Accordingly, after extraction of the numerical simulation's results in this section, the Reynolds stresses including $\tau_{u'w'}$ and $\tau_{v'w'}$ parameters along the flow depth for station $X/L = 0.5$ are discussed (Figure 8).

In the region near the bed with A-Jacks armor, the Reynolds shear stresses $\tau_{u_l w_l}$ and $\tau_{v_l w_l}$ from the channel bed increase. Then, further away from the bed in $Y/Y_t = 0.5 - 1.5$ region, the Reynolds shear stresses of $\tau_{u_l w_l}$ and $\tau_{v_l w_l}$ reach their maximum. Afterwards, in $Y/Y_t = 2 - 10$ region, the Reynolds shear stresses $\tau_{u_l w_l}$ and $\tau_{v_l w_l}$ decrease to near-zero values at the water surface. Near-zero values close to the water surface suggest highly low shear in this region and the effect of free surface. This means that the shear stress is minimum at a layer near the water surface, and the geometry of A-Jacks armors has not been able to affect the free water surface at this layer. In other words, although increasing A-Jacks armors' dimensions entails an increase in the Reynolds shear stress parameters, it does not have much effect along the flow depth. According to the presented diagram, the maximum Reynolds shear stress values occurred in a region farther away from the bed, the result of which is that the shear stress in the vicinity of sediment particles at the layer beneath the armor is zero; therefore, it can play a significant part in reducing scour in these regions.

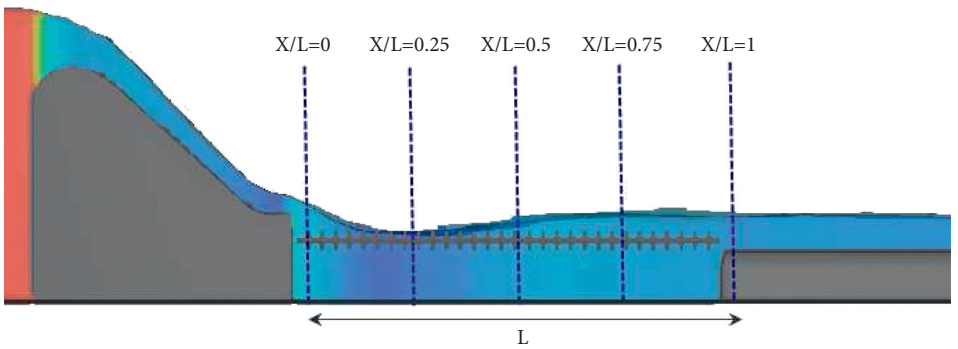

Figure 6: Side view of the numerical model and the properties of the stations measuring flow hydrodynamic parameters.

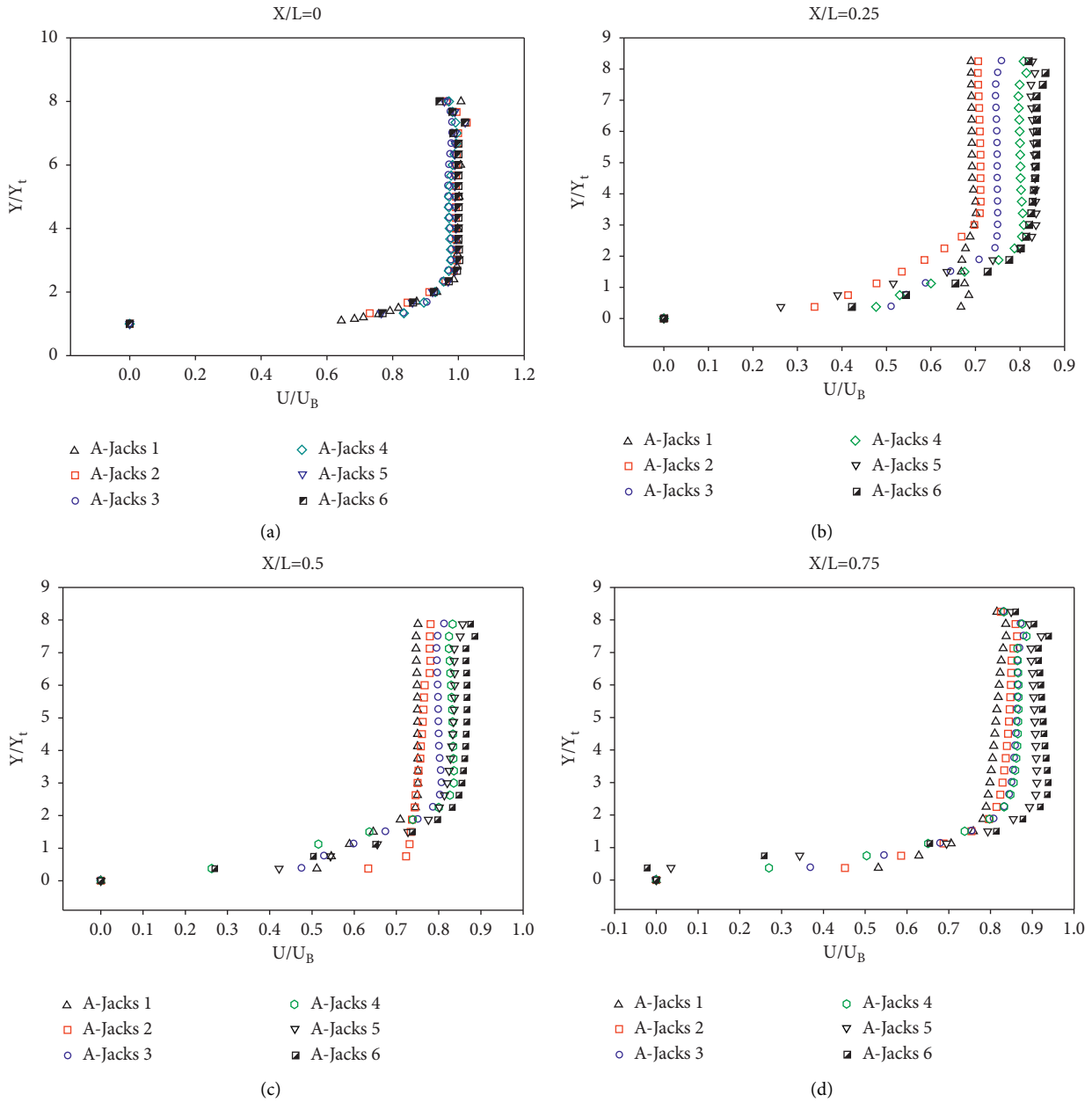

Figure 7: Continued.

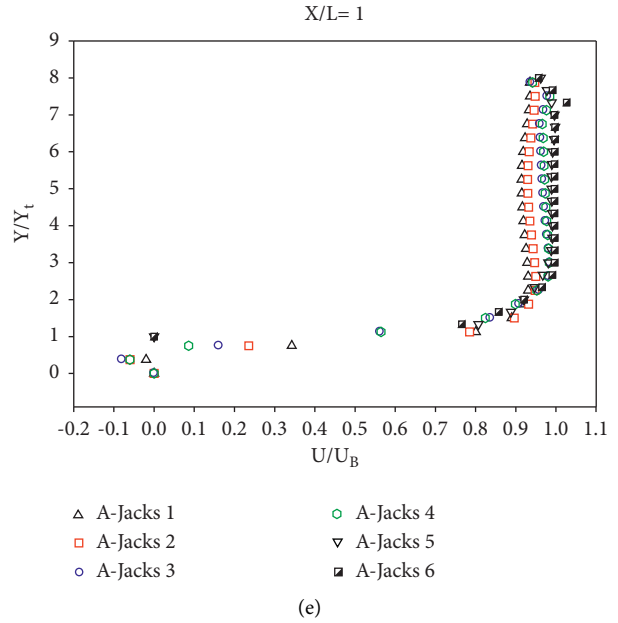

Figure 7: Velocity profiles at station (X/L = 0, 0.25, 0.5, 0.75, 1) downstream of the flip bucket with A-Jacks (1 to 6).

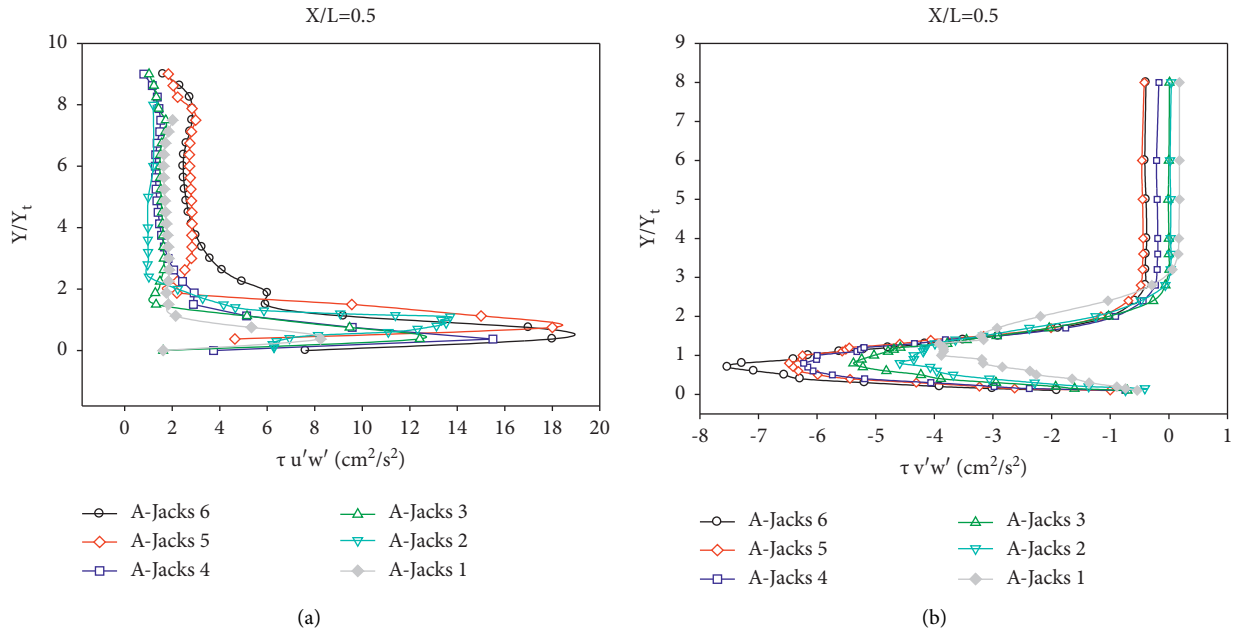

Figure 8: Reynolds shear stress profiles of $\tau_{u'w'}$ and $\tau_{v'w'}$ for station X/L = 0.5.

A-Jacks armors have 6 interlocked piers, which cause great roughness at bed. Due to creation of roughness at bed, when the flow is passing over the rough bed, the adhesive drag force functions as the main inhibitor against the flow [29]. In rough beds similar to A-Jacks armors, the skin friction coefficient (C_f) is put forth for measuring resistance against the flow. The skin friction coefficient (C_f) along the flow length has been extracted for 6 modes of A-Jacks armors using the simulations, and it is shown in Figure 9.

As shown in Figure 9, with the impact of the jet with A-Jacks armor, skin friction coefficient (C_f) values are highly varied due to great turbulence resulting from the impact of the jet with the tailwater. Since the shear stress values parameters ($C_f = 2[u_*/U]^2$) and the flow velocity are involved in the skin friction coefficient (u_*) equation, the shear velocity values could increase along the flow length and entail an increase in the skin friction coefficient (C_f) values. The results of the numerical model indicate that with an increase in the size of A-Jacks armors, vortex flows between the piers lead to a decrease in the resulting flow energy. Along A-Jacks armors, the elements' roughness affects both the friction force and the

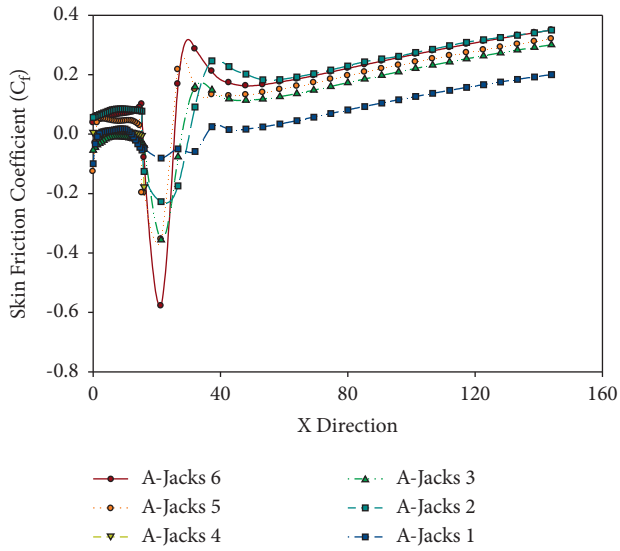

Figure 9: . Skin friction coefficient (C_f) along the flow length for 6 modes of A-Jacks armors.

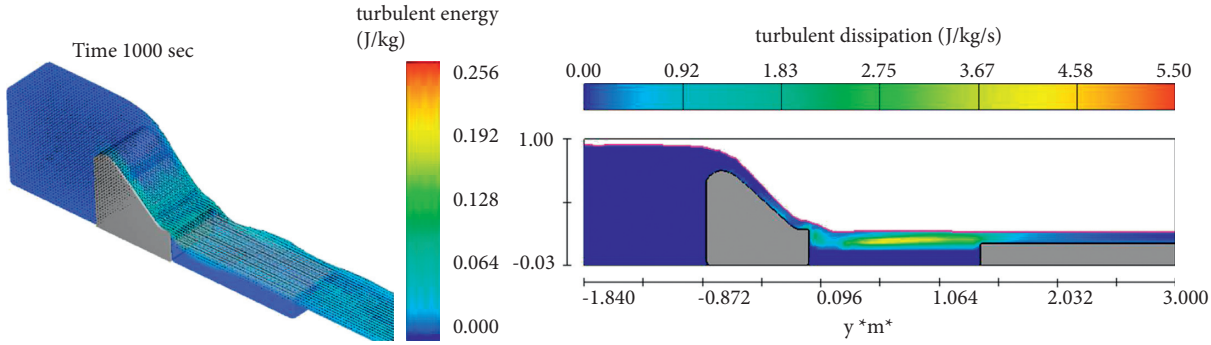

Figure 10: Flow turbulence energy variations and flow turbulence energy dissipation downstream of flip buckets.

compressive drag force from the fluid on the bed. Under the same hydraulic conditions, the compressive drag force increases as much as the elements become larger, and the overall force imposed on the flow will be larger, leading to an increase in energy loss. The parameters of the flow turbulence energy values and the flow turbulence energy dissipation extracted from the Flow3D numerical model are depicted in Figure 10. Increase in flow turbulence energy dissipation downstream of flip buckets significantly mitigates the conditions of scour occurrence and confirms the proper performance of A-Jacks armors in reducing scour depth.

5. Conclusion

Regarding the extensive use of flip buckets in chute spillways, particularly in major (concrete or embankment) dams, it is regarded important to build and analyze a bed protection system for this type of dissipater's tailwater. Accordingly, this study analyzed the hydrodynamic parameters of the A-Jacks bed protective system. The bed erosion mechanism downstream of flip buckets is made analyzable by determining the flow hydrodynamic parameters. Due to flow jet turbulence, there are vortices developed in the region near the bed and the region downstream of the flip bucket jet that can play an important role in digging, lifting, and transporting sediments. As the numerical model results indicated, utilizing A-Jacks armors could entail desirable variations in flow velocity profiles U/U_B, Reynolds stresses $\tau_{u'w'}$ and $\tau_{v'w'}$, and the skin friction coefficient C_f. The size of A-Jacks elements can have a role in increasing the flow turbulence to a certain depth so that after the impact of the flow with A-Jacks armor, the vortices' intensity as well as the shear stress affecting the bed gradually decreases because first the water depth values at the tailwater are increased locally and then the excessive flow energy is dissipated due to the armor's roughness. As a result of this process, the shear stress values and the vortices' intensity decrease. Altogether, the numerical model results suggest that A-Jacks armors enjoy highly proper geometric conditions which can improve the flow hydrodynamic conditions downstream of flip buckets towards reducing bed erosion to a very significant extent.

Data Availability

All data used to support the findings of the study are included within the article.

Conflicts of Interest

The authors declare that there are no conflicts of interest regarding the publication of this paper.

References

[1] Report MHL 1251, "Physical modelling of a-jacks units in wave flume," Report No. MHL1251, Manly Hydraulics Laboratory, Manly Vale, Australia, 2003.

[2] C. I. Thornton, C. C. Watson, S. R. Abt, C. M. Lipscomb, and C. M. Ullman, *Laboratory Testing of A-JACKS Units for Inland Applications: Pier Scour Protection Testing*, Colorado State University research report for Armortec Inc., Collins, CO, USA, 1999.

[3] J. J. Mickel, "A-jacks matrix stability: deflection due to static normal loads," M.Sc. Thesis, Oregon State University, Corvallis, OR, USA, 1999.

[4] T. E. Latta, "Static and dynamic stresses in a-jacks concrete armor units," M.Sc. Thesis, Oregon State University, Corvallis, OR, USA, 2000.

[5] M. Zolghadr and M. Shafai Bejestan, "Six legged concrete (SLC) elements as scour countermeasures at wing wall bridge abutments," *International Journal of River Basin Management*, vol. 1, pp. 1–7, 2020.

[6] M. Zolghadr, M. S. Bejestan, and M. Rezaeianzadeh, "Investigating the effect of six-legged element placement density on local scour at wing-wall bridge abutments," in *Proceedings of the World Environmental and Water Resources Congress 2016*, West Palm Beach, FL, USA, May 2016.

[7] H. Reza, A. Ali, M. S. Bajestan, M. Ghomeshi, and M. Fathi Moghadam, "Investigation of the effect of six legged concrete (SLC) elements combined with riprap on scour depth at vertical wall bridge abutments," *Irrigation Sciences and Engineering*, vol. 42, no. 1, pp. 99–114, 2019.

[8] K. Khalifehei, G. Azizyan, M. Shafai-Bajestan, and K.-w. Chau, "Stability of A-Jack concrete block armors protecting the riverbeds," *Ain Shams Engineering Journal*, vol. 12, no. 1, pp. 381–391, 2021.

[9] K. Khalifehei, G. Azizyan, M. Shafai-Bajestan, and K. W. Chau, "Experimental modeling and evaluation sediment scouring in riverbeds around downstream in flip buckets," *International Journal of Engineering*, vol. 33, no. 10, pp. 1904–1916, 2020.

[10] M. R. Nou, M. A. Moghaddam, M. S. Bajestan, and H. M. Azamathulla, "Control of bed scour downstream of ski-jump spillway by combination of six-legged concrete elements and riprap," *Ain Shams Engineering Journal*, vol. 11, pp. 1047–1059, 2020.

[11] H. Vaseli, L. Hashemian, and A. Bayat, "Productivity analysis of micro-trenching using simphony simulation modeling," *Civil Engineering Journal*, vol. 6, no. 11, pp. 2131–2142, 2020.

[12] C. W. Hirt and B. Nichols, "Flow-3D User's manual," *Flow Science Inc*, vol. 107, 1988.

[13] N. J. H. Al-Mansori, L. S. A. Al-Zubaidi, and Al-Zubaidi Laith Shaker Ashoor, "One-dimensional hydrodynamic modeling of the euphrates river and prediction of hydraulic parameters," *Civil Engineering Journal*, vol. 6, no. 6, pp. 1074–1090, 2020.

[14] A. Yamini, S. H. M. Omid, M. R. Kavianpour, and Ramin Safari Ghaleh, "Hydrodynamic performance and cavitation analysis in bottom outlets of dam using CFD modelling," *Advances in Civil Engineering*, vol. 2021, Article ID 5529792, 14 pages, 2021.

[15] S. M. Mousavimehr, Omid Aminoroayaie Yamini, and M. R. Kavianpour, "Performance assessment of shockwaves of chute spillways in large dams," *Shock and Vibration*, vol. 2021, Article ID 6634086, 17 pages, 2021.

[16] A. Anand, M. Beg, and N. Kumar, "Experimental studies and analysis on mobilization of the cohesionless sediments through alluvial channel: a review," *Civil Engineering Journal*, vol. 7, no. 5, pp. 915–936, 2021.

[17] A. Temel and D. Mustafa, "Time dependent investigation of the wave induced scour at the trunk section of a rubble mound breakwater," *Ocean Engineering*, vol. 221, Article ID 108564, 2021.

[18] G. Mihajlović and M. Živković, "Sieving extremely wet earth mass by means of oscillatory transporting platform," *Emerging Science Journal*, vol. 4, no. 3, pp. 172–182, 2020.

[19] A. Movahedi, M. R. Kavianpour, and Omid Aminoroayaie Yamini, "Evaluation and modeling scouring and sedimentation around downstream of large dams," *Environmental Earth Sciences*, vol. 77, no. 8, pp. 1–17, 2018.

[20] B. Fazelabdolabadi and M. H. Golestan, "Towards bayesian quantification of permeability in micro-scale porous structures-the database of micro networks," *HighTech and Innovation Journal*, vol. 1, no. 4, pp. 148–160, 2020.

[21] M. Nazari-Sharabian, M. Karakouzian, M. Karami, and M. Karami, "Sacrificial piles as scour countermeasures in river bridges a numerical study using FLOW-3D," *Civil Engineering Journal*, vol. 6, no. 6, pp. 1091–1103, 2020.

[22] Helbar, M. Sadat, Atefeh Parvaresh Rizi, J. Farhoudi, and A. Mohammadi, "3D flow simulation to improve the design and operation of the dam bottom outlets," *Arabian Journal of Geosciences*, vol. 14, no. 2, pp. 1–11, 2021.

[23] K. Khosravi, Z. S. Khozani, and L. Mao, "A comparison between advanced hybrid machine learning algorithms and empirical equations applied to abutment scour depth prediction," *Journal of Hydrology*, vol. 596, Article ID 126100, 2021.

[24] V. Yakhot, S. A. Orszag, S. Thangam, T. B. Gatski, and C. G. Speziale, "Development of turbulence models for shear flows by a double expansion technique," *Physics of Fluids*, vol. 4, no. 7, pp. 1510–1520, 1992.

[25] V. Zhaba and E. Gohman, "Activation level and probabilities of electromagnetic γ-transitions in the reaction 77Se (γ, γ') 77mSe," *Emerging Science Journal*, vol. 4, no. 3, pp. 165–171, 2020.

[26] K. Khalifehei, G. Azizyan, and C. Gualtieri, "Analyzing the performance of wave-energy generator systems (SSG) for the southern coasts of Iran, in the Persian gulf and Oman sea," *Energies*, vol. 11, no. 11, p. 3209, 2018.

[27] S. B. Dirbude and V. K. Maurya, "Effect of uniform magnetic field on melting at various Rayleigh numbers," *Emerging Science Journal*, vol. 3, no. 4, pp. 263–273, 2019.

[28] A. Movahedi, M. Kavianpour, and O. Aminoroayaie Yamini, "Experimental and numerical analysis of the scour profile downstream of flip bucket with change in bed material size," *ISH Journal of Hydraulic Engineering*, vol. 25, no. 2, pp. 188–202, 2019.

[29] R. Fernández, A. J. Vitale, G. Parker, and M. H. García, "Hydraulic resistance in mixed bedrock-alluvial meandering channels," *Journal of Hydraulic Research*, vol. 59, no. 2, pp. 298–313, 2021.